for the cobalt(II) complex[3] and ~8 kJ mol^{-1} in electrostatic work terms). Thus the observed $k_{-a} = 5 \times 10^5$ M^{-1} s^{-1} is somewhat smaller than the expected diffusional limit (~10^7 M^{-1} s^{-1}),[27c] and there appears to be a small ($\Delta G_r^{\ddagger} \approx 9$ kJ mol^{-1}) activation barrier to combination of the reactant pair in the solvent cage.[28]

In general, the activation free energy of a reaction depends on certain intrinsic components $\Delta G_i^{\ddagger}$, modified by the driving force of the reaction, $\Delta G°$. A general functional dependence, $\Delta G^{\ddagger} = \alpha \Delta G° + \Delta G_i^{\ddagger}(M(\alpha))$, has been suggested for group-transfer reactions,[29,30] where α is the Brønsted coefficient and $M(\alpha)$ is some function of α. For small values of $\Delta G°$ this should reduce to $\Delta G^{\ddagger} \simeq {}^1/_2 \Delta G° + \Delta G_i^{\ddagger}$. This approach has been useful in obtaining intrinsic parameters for inner-sphere electron-transfer reactions.[27] Application in the present system, to correct $\Delta G_r^{\ddagger}$ for the free energy change implies that $\Delta G_i^{\ddagger} \approx 25$ kJ mol^{-1}. A significant intrinsic barrier to adduct formation is very reasonable considering the magnitude of bond length changes which must occur at the Co^{II}[3] and O_2 centers.[4,21,22,31] It may be expected that future work will elucidate the nature of this barrier.

Registry No. $\{[H_2OCo([14]aneN_4)]_2O_2\}(ClO_4)_4$, 15661-33-3; $[H_2OCo(Me_2[14]4,11\text{-}dieneN_4)]_2O_2^{4+}$, 58880-97-0; $[Co([14]aneN_4)Cl_2]ClO_4$, 15220-75-4; $[Co([14]aneN_4)O_2HCl]ClO_4$, 77495-52-4; $Fe(bpy)_3^{3+}$, 18661-69-3; Ce^{4+}, 16065-90-0; $Co(Me_4[14]tetraeneN_4)Cl_2^+$, 43225-24-7; Fe^{3+}, 20074-52-6; Fe^{2+}, 15438-31-0; $S_2O_8^{2-}$, 15092-81-6; $Ru(NH_3)_5py^{2+}$, 21360-09-8; Cr^{2+}, 22541-79-3; $Co(Me_4[14]tetraeneN_4)(OH_2)_2^{2+}$, 38337-82-5; $Co([14]aneN_4)(H_2O)_2^{2+}$, 65554-13-4; $Fe(phen)_3^{3+}$, 13479-49-7; H_2O_2, 7722-84-1.

Supplementary Material Available: Figures of the temperature dependence of μ-peroxo decomposition in $HClO_4$, pH changes accompanying μ-peroxo decomposition in NaCl, and oxygen dependence of μ-peroxo decomposition and tables showing oxygen uptake or release during oxidations or reductions of $[H_2OCo([14]aneN_4)]_2O_2^{4+}$ in aerated solutions, rate constants for oxidations of $[H_2OCo([14]aneN_4)]_2O_2^{4+}$, oxygen released in reactions of $[H_2OCo([14]aneN_4)]_2O_2^{4+}$ with oxidants in deaerated solutions, rate constants for reductions of $[H_2OCo([14]aneN_4)]_2O_2^{4+}$, $[Fe^{3+}]$ produced in $Fe^{2+}/[H_2OCo([14]aneN_4)]_2O_2^{4+}$ reactions, oxygen uptake in $Fe^{2+}/[H_2OCo([14]aneN_4)]_2O_2^{4+}$ reactions, and rate constants for reactions of $Co^{II}([14]aneN_4)$ (23 pages). Ordering information is given on any current masthead page.

(27) Similar considerations apply to any "inner-sphere" reaction. For example see: (a) Endicott, J. F.; Wong, C. L.; Ciskowski, J. C.; Balakrishnan, K. P. *J. Am. Chem. Soc.* **1980**, *102*, 2100. (b) Endicott, J. F.; Balakrishnan, K. P.; Wong, C. L. *Ibid.* **1980**, *102*, 5519. (c) Durham, B.; Endicott, J. F.; Wong, C. L.; Rillema, D. P. *Ibid.* **1979**, *101*,

(28) For comparison, combination of the adenosyl radical with a cob(II)-alamin fragment in a solvent cage has an apparent activation barrier of nearly 5 kcal mol^{-1}: Endicott, J. F.; Netzel, T. L. *J. Am. Chem. Soc.* **1979**, *101*, 4000.

(29) Marcus, R. A. *J. Phys. Chem.* **1968**, *72*, 891.

(30) Levine, R. D. *J. Phys. Chem.* **1979**, *83*, 159.

(31) Endicott, J. F.; Lilie, J.; Kuszaj, J. M.; Ramaswamy, B. S.; Schmonsees, W. G.; Rillema, D. P. *J. Am. Chem. Soc.* **1977**, *99*, 429.

Contribution from the Department of Organic Synthesis, Faculty of Engineering, Kyushu University, Fukuoka 812, Japan

Transition-Metal Complexes of Pyrrole Pigments. 18. Redox Behaviors of Oxomolybdenum(V) Complexes Formed with Macrocyclic Tetrapyrroles

YOSHIHISA MATSUDA, SUNAO YAMADA, and YUKITO MURAKAMI*

Received July 7, 1980

The redox chemistry of (2,3,17,18-tetramethyl-7,8,12,13-tetraethylcorrolato)oxomolybdenum(V) [Mo(O)(MEC)] and (5,10,15,20-tetraphenylporphinato)oxomolybdenum(V) complexes [Mo(O)(TPP)(X), X = MeO, AcO, and Cl] was investigated in dichloromethane by means of cyclic voltammetry and controlled-potential electrolysis. One-electron oxidation and reduction of Mo(O)(MEC) at Mo^V were observed at +0.70 and −0.72 V vs. SCE, respectively. Such oxidation and reduction potentials for Mo(O)(TPP)(X) were very dependent on the nature of axial ligand X and consequently on the covalent character of the Mo^V–X bond: one-electron reduction becomes less facile as the covalent character increases and reaches the value of that in Mo(O)(MEC) for X = MeO. The TPP complexes were much more resistant to oxidation of Mo^V than the MEC complex. Two successive reductions of TPP were observed for Mo(O)(TPP)(X) at −1.1 and −1.5 V vs. SCE while no ligand reduction was detected for Mo(O)(MEC) in the cathodic region up to −2.0 V vs. SCE. On the basis of complete redox schemes for Mo(O)(MEC) and Mo(O)(TPP)(X), correlations between redox properties and ligand structures have been discussed. Coordination equilibria for reactions of Mo(O)(TPP)(MeO) with AcO^-, Cl^-, and ClO_4^- were investigated in dichloromethane, and the chloro complex was found to exist as a dimer while the others are monomers in solution.

Introduction

Several molybdenum(V) complexes of macrocyclic tetrapyrroles such as corrole and porphyrins have been prepared and characterized by various physical methods.[1-9] The molybdenum ion has been known to show strong affinity for oxygen in its higher oxidation states (+4 to +6), and pentavalent molybdenum complexes having an oxo group have been isolated as the most stable ones. Thus, porphyrin complexes involving tetra- and hexavalent molybdenum have been prepared from the pentavalent complexes by using appropriate oxidizing or reducing agents.[10-12] As a step toward preparation of one-dimensional electric conductors by stacking planar metal complexes with the formation of metal–metal bonds, molybdenum complexes of macrocyclic tetrapyrroles are plausible ones for this purpose since the metal ion has a strong tendency to form metal to metal bonds in its low oxidation states. The redox behaviors of molybdenum complexes need to be investigated in order to obtain chemical conditions

(1) Srivastava, T. S.; Fleischer, E. B. *J. Am. Chem. Soc.* **1970**, *92*, 5528.
(2) Fleischer, E. B.; Srivastava, T. S. *Inorg. Chim. Acta* **1971**, *5*, 151.
(3) Buchler, J. W.; Puppe, L.; Rohbock, K.; Schneehage, H. H. *Chem. Ber.* **1973**, *106*, 2710.
(4) Murakami, Y.; Matsuda, Y.; Yamada, S. *Chem. Lett.* **1977**, 689.
(5) Matsuda, Y.; Kubota, F.; Murakami, Y. *Chem. Lett.* **1977**, 1281.
(6) Ledon, H.; Mentzen, B. *Inorg. Chim. Acta* **1978**, *31*, L393.
(7) Hayes, R. G.; Scheidt, W. R. *Inorg. Chem.* **1978**, *17*, 1082.
(8) Johnson, J. F.; Scheidt, W. R. *Inorg. Chem.* **1978**, *17*, 1280.
(9) Ohta, N.; Scheuermann, W.; Nakamoto, K.; Matsuda, Y.; Yamada, S.; Murakami, Y. *Inorg. Chem.* **1979**, *18*, 457.

(10) Chevrier, B.; Diebold, Th.; Weiss, R. *Inorg. Chim. Acta* **1976**, *19*, L57.
(11) Diebold, Th.; Chevrier, B.; Weiss, R. *Angew. Chem.* **1977**, *89*, 819.
(12) Diebold, Th.; Chevrier, B.; Weiss, R. *Inorg. Chem.* **1979**, *18*, 1193.

0020-1669/81/1320-2239$01.25/0

for the formation of molybdenum complexes in low valency states with use of pentavalent complexes as parent materials.

Redox properties of molybdenum(V) porphyrin complexes have been reported previously by Davis et al.[13,14] but poorly characterized. On the other hand, the redox chemistry of molybdenum(V) corrole has never been investigated before. A significant structural difference between corrole and porphyrin is that the former has a direct linkage between A and D pyrrole rings while the latter has a methylene group between the rings. The direct A–D linkage may cause deformation of the macrocyclic skeleton so that the four pyrrole rings cannot stay on the same plane. Corrole coordinates to metal ions as a trinegative ligand while porphyrin as a dinegative one. Since the structural feature of corrole is somewhat different from that of porphyrin, it is of interest to correlate redox behaviors of their molybdenum complexes with ligand structures.

We have investigated in the present work the redox properties of pentavalent molybdenum complexes of 2,3,17,18-tetramethyl-7,8,12,13-tetraethylcorrole (abbreviated as MEC for a trinegative anion) and 5,10,15,20-tetraphenylporphine (abbreviated as TPP for a dinegative anion) by cyclic voltammetry and controlled-potential electrolysis. The pentavalent molybdenum forms TPP complexes as Mo(O)(TPP)(X), where X^- stands for methoxo, acetato, or chloro

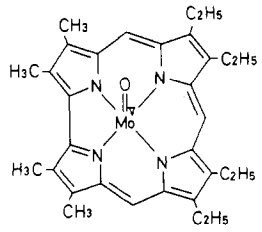

Mo(O)(MEC)

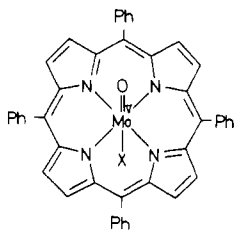

Mo(O)(TPP)(X)
X=OMe,OAc,Cl

group. Coordination equilibria for reactions of Mo(O)(TPP)(MeO) with such monoanionic ligands have also been examined.

Experimental Section

Materials. Dichloromethane was purified by the standard procedure[15] and kept over a molecular sieve (3A, Ishizu Pharmaceutical Co.). Tetrabutylammonium perchlorate (TBAP) of polarographic grade and tetraethylammonium chloride (TEAC) of guaranteed reagent grade were obtained from Nakarai Chemicals and Wako Pure Chemicals, respectively, and used without further purification.

(2,3,17,18,-Tetramethyl-7,8,12,13-tetraethylcorrolato)oxomolybdenum(V) [Mo(O)(MEC)] has been prepared as described previously[4] [μ_{eff}(296.9 K) 1.649 μ_B].

Methoxo(5,10,15,20-tetraphenylporphinato)oxomolybdenum(V) [Mo(O)(TPP)(MeO)] has been obtained by a method similar to that reported previously:[5] IR(Nujol mull) 906 (Mo=O str), 474 (Mo—O str.) cm^{-1}; μ_{eff}(290.7 K) 1.591 μ_B. Anal. Calcd for $C_{45}H_{31}MoN_4O_2$: C, 71.52; H, 4.13; N, 7.41. Found: C, 71.82; H, 4.31; N, 7.11.

Acetato(5,10,15,20-tetraphenylporphinato)oxomolybdenum(V) [Mo(O)(TPP)(AcO)]. A 100-mg sample of Mo(O)(TPP)(MeO) was dissolved in 25 mL of acetic acid–dichloromethane (4:1 v/v) and refluxed for 3 h. After the solution was evaporated to dryness in vacuo at room temperature, the solid residue was dissolved in 5 mL of acetic acid and allowed to stand in a freezer overnight. Developed dark green precipitates were collected, washed with 100 mL of acetic acid–hexane (1:9 v/v), and dried in vacuo at 80 °C: yield 72 mg (69%); IR(Nujol mull), 942, 919 (Mo=O str), 480 cm^{-1} (Mo—O str); μ_{eff}(301.2 K) 1.697 μ_B. Anal. Calcd for $C_{46}H_{31}MoN_4O_3$: C, 70.50; H, 3.99; N, 7.15. Found: C, 69.92; H, 4.02; N, 6.97. The complex was also obtained from $[Mo(O)(TPP)]_2O$[3] by a similar procedure.

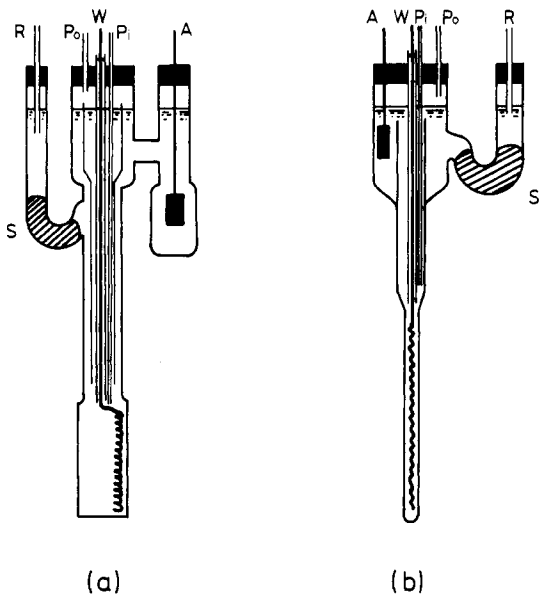

Figure 1. Three-electrode cells for controlled-potential electrolysis as followed by electronic (a) and ESR (b) spectroscopy: A, auxiliary electrode; P_i, inert gas inlet; P_o, inert gas outlet; R, reference electrode (SCE); S, salt bridge; W, working electrode (platinum wire).

Chloro(5,10,15,20-tetraphenylporphinato)oxomolybdenum(V) [Mo(O)(TPP)Cl]. A solution of Mo(O)(TPP)(MeO) (50 mg) in 15 mL of dichloromethane was added dropwise to 60 mL of hexane saturated with dry hydrogen chloride at room temperature. The resulting crystalline solid was collected and washed with 70 mL of hexane to give fine dark green crystals: yield 40 mg (80%); IR(Nujol mull) 939 cm^{-1} (Mo=O str). Anal. Calcd for $C_{44}H_{28}ClMoN_4O$: C, 69.53; H, 3.71; N, 7.37. Found: C, 68.44; H, 4.04; N, 6.83. The complex was also obtained from $[Mo(O)(TPP)]_2O$ by a similar procedure.

Spectroscopic Measurements. Electronic absorption spectra covering the 350–800-nm range were recorded on a Union Giken SM-401 spectrophotometer. ESR spectra were obtained on a JEOL JES-ME-3 X-band spectrometer equipped with 100-kHz field modulation unit; a standard MgO/Mn^{II} sample calibrated with a NMR magnetometer was employed for calibration of the magnetic field.

Electrochemical Measurements. Cyclic voltammetry was carried out on a YANACO P-8 polarograph equipped with the combination of a TOA HP-105 platinum and a Metrohm EA-211b platinum electrode as working and auxiliary electrodes, respectively. A saturated calomel electrode (SCE) was served as a reference which was separated from a bulk electrolyte solution by a salt bridge prepared with agar and saturated aqueous potassium chloride; glass filters were doubly inserted between the salt bridge and the bulk solution to minimize the diffusion of water into the latter.[16] A dichloromethane solution containing a molybdenum complex (5.0×10^{-4} M) and TBAP (5.0×10^{-2} M) was deaerated prior to each measurement, and the inside of the cell was maintained under argon atmosphere throughout each measurement. All the measurements were carried out at 25 ± 2 °C for Mo(O)(TPP)(X) and at 18 °C for Mo(O)(MEC). The scan rate was varied in a range from 5 to 500 mV s^{-1}.[17] Half-wave potentials ($E_{1/2}$) and anodic (i_{pa}) and cathodic (i_{pc}) currents were evaluated for

(13) Fuhrhop, J.-H.; Kadish, K. M.; Davis, D. G. *J. Am. Chem. Soc.* **1973**, *95*, 5140.
(14) Newton, C. M.; Davis, D. G. *J. Magn. Reson.* **1975**, *20*, 446.
(15) Riddick, J. A.; Bunger, W. B. "Organic Solvents"; Wiley-Interscience: New York, 1970.

(16) When a Ag/AgCl reference electrode with aqueous tetraethylammonium chloride as a salt bridge was used, electrochemical behaviors of the complexes were identical with those observed here with a combination of SCE–KCl salt bridge at scan rates in a range of 5–200 mV s^{-1}. Unsatisfactory agreement between the electrochemical behaviors observed with the above two reference systems at higher scan rates (>200 mV s^{-1}) is primarily due to an insufficient compensation of the cell impedance in the latter system.

(17) The use of a scan rate as high as 500 mV s^{-1} would require greater concentrations of a supporting electrolyte (>5.0×10^{-2} M) since a plot of a value of $i_{pa} + i_{pc}$ vs. $v^{1/2}$ slightly deviates from the linear correlation for reversible electron-transfer processes. Consequently, the electrochemical data were obtained from observations at scan rates in a range of 5–100 mV s^{-1}.

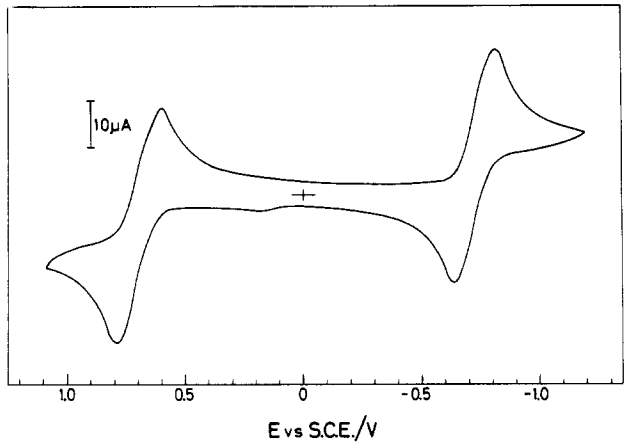

Figure 2. Cyclic voltammogram of Mo(O)(MEC) (5.0×10^{-4} M) in dichloromethane containing 5.0×10^{-2} M TBAP at 18 °C (scan rate 100 mV s^{-1}).

Table I. Spin Hamiltonian Parameters for Mo(V) Complexes in Dichloromethane at Room Temperature

complex[a]	g	$10^4 A_{Mo}$, cm^{-1}	$10^4 A_N$, cm^{-1}	ref
Mo(O)(MEC)	1.967	41.8	2.3	4
Mo(O)(TPP)(MeO)	1.964	45.2	2.3	this work
Mo(O)(TPP)(AcO)	1.961	48.5	2.4	this work
Mo(O)(TPP)(MeO) + HCl gas	1.961	43.4	2.4	this work

[a] Concentrations of the complexes ca. 10^{-3} M.

the data obtained at scan rates of 5–100 mV s^{-1}, by referring to the literature methods.[18]

Controlled-potential electrolysis was carried out in a three-electrode cell, modified for ESR and electronic absorption measurements, with platinum wire of 0.5-mm diameter as a working electrode (Figure 1). The auxiliary and reference electrodes were the same as used for voltammetric measurements. An applied potential between the working and auxiliary electrodes was maintained constant with a conventional potentiostat and monitored with a Takeda Riken TR-6656 digital multimeter.

Results

Electrochemical Behavior of Mo(O)(MEC). A typical cyclic voltammogram for Mo(O)(MEC) is shown in Figure 2, where two redox couples are observed at 0.70 and −0.72 V vs. SCE in a potential range from 1.1 to −2.0 V. The ratios between anodic and cathodic peak currents, i_{pa}/i_{pc}, were unity and independent of scan rate (from 5 to 100 mV s^{-1}) for the two redox couples. Plots of i_p ($=i_{pa} + i_{pc}$) vs. $v^{1/2}$ (v for scan rate, mV s^{-1}) were linear, and potential separation between the anodic and cathodic peaks varied from 180 to 90 mV for the two redox couples, while $E_{1/2}$ values were constant within an accuracy of ±3% regardless of scan rate variation. We refer, therefore, each redox process to reversible one-electron transfer without any coupled chemical reaction.[18] The one-electron oxidation and/or reduction products were examined by pursuing controlled-potential electrolysis of the complex by ESR spectroscopy. Spin Hamiltonian parameters for the Mo^V complexes of our present concern are listed in Table I.

A dichloromethane solution of $Mo^V(O)(MEC)$ (10^{-3} M) was electrochemically reduced in the presence of 0.1 M TBAP at −1.0 V vs. SCE. ESR signal intensity of the parent complex decreased with time and completely disappeared after 2.5 h of electrolytic reduction without observing any new signal. The ESR signal was recovered immediately by interrupting the reduction then. This reversible one-electron redox reaction

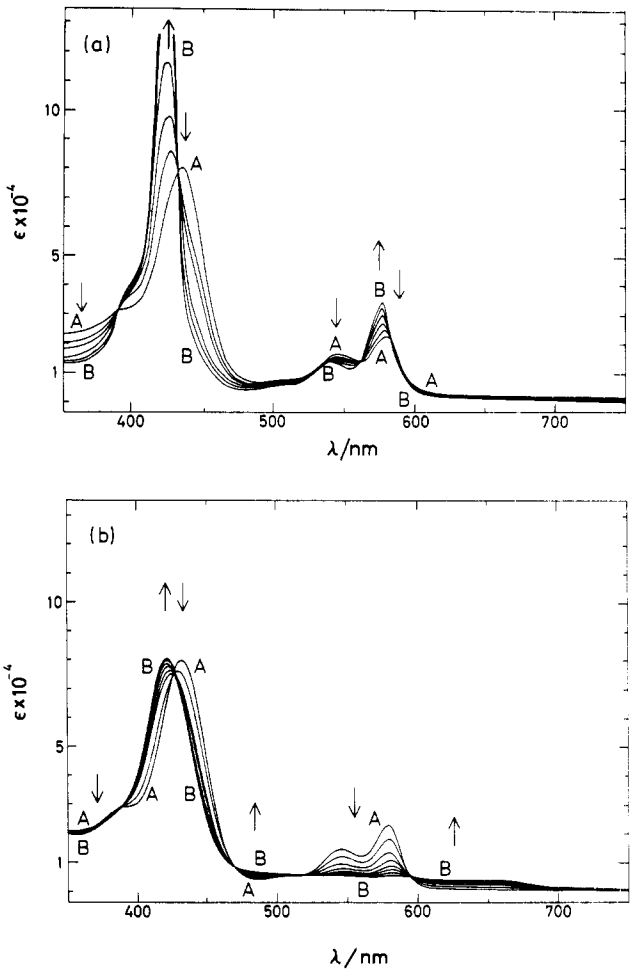

Figure 3. Electrochemical reduction (at −1.0 V vs. SCE) and oxidation (at 1.0 V vs. SCE) of Mo(O)(MEC) (1.5×10^{-5} M) in dichloromethane containing 5.0×10^{-2} M TBAP at 15 °C: (a) A, Mo^V(O)(MEC); B, one-electron-reduced species; (b) A, Mo^V(O)(MEC); B, one-electron-oxidized species. Trends of spectral changes with time are shown by arrows.

must, therefore, occur at the central metal atom: Mo^V/Mo^{IV}. The chemical reduction of Mo(O)(MEC) was carried out with sodium benzophenone ketyl in dichloromethane–pentane (2:1 v/v); the resulting solution did not show any ESR signal for a temperature range from 77 K to room temperature. These results are in accord with the formation of Mo^{IV} species, $[Mo^{IV}(O)(MEC)]^-$ ion, and exclude the possible formation of a Mo^V species in triplet spin state, $[Mo^V(O)(MEC^{-\cdot})]^-$ ion. Likewise, Mo(O)(MEC) showed a change in electronic spectrum as the electrolytic reduction proceeded in dichloromethane, having well-defined isosbestic points at 392, 430, 560, and 583 nm (Figure 3a). The monoanionic species, however, decomposed slowly during a prolonged reaction time, and ca. 80% of the original complex was recovered by electrolytic reoxidation at 0 V vs. SCE. The spectrum of the electrochemically reduced species was sufficiently identical with that of the chemically reduced one. The reduction product obtained by the latter process was stable at least for 1 h under anaerobic conditions. About 80% of the original Mo^V complex was converted to $[Mo^{IV}(O)(MEC)]^-$ electrochemically in reference to the absorption intensity of the chemical reduction product.

Oxidation of Mo(O)(MEC) in dichloromethane was performed electrochemically at +1.0 V vs. SCE, and the ESR signal due to the Mo^V species decreased as the reaction proceeded, the one-electron oxidation of molybdenum (Mo^{VI}/Mo^V) taking place. The electrolytic oxidation process was followed clearly by electronic spectroscopy as shown in Figure

(18) Adams, R. "Electrochemistry at Solid Electrodes"; Marcel Dekker: New York, 1969; pp 143–162.

Scheme I

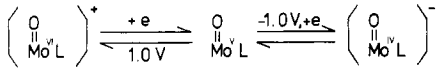

L : MEC

Table II. Electronic Absorption Bands (nm) for H_3MEC, Mo(O)(MEC), and Reduced and Oxidized Mo(O)(MEC) in Dichloromethane[a]

H_3MEC	Mo(O)(MEC)	$[Mo(O)(MEC)]^-$ [b]	$[Mo(O)(MEC)]^+$ [c]
399 (117)	388 sh (29.5)	368 sh (19.1)	419 (81.0) (S)
407 (94.8)	432 (79.5) (S)	393 (40.5)	522 sh (5.24)
480 sh (5.0)	501 sh (5.23)	419 (187) } (S)	596 (3.97) (β)
505 sh (6.7)	543 (13.8) (β)	424 sh (170) }	648 (4.02) (α)
538 (13.8)	577 (21.9) (α)	500 (3.27)	
553 (13.3)		537 (12.5) (β)	
595 (14.8)		566 sh (27.2) } (α)	
		575 (43.2) }	

[a] Measured at 15 °C in the presence of TBAP (5.0×10^{-2} M); molar absorption coefficients are given in parentheses after absorption bands as $\epsilon \times 10^{-3}$ (M^{-1} cm^{-1}); S, α, and β in parentheses stand for Soret, α, and β bands, respectively. [b] Reduced with sodium benzophenone ketyl. [c] Oxidized with $FeCl_3$.

3b, where isosbestic points are at 387, 426, 468, 516, and 593 nm. Since the electrolytic rereduction of the oxidized species at 0 V vs. SCE resulted in regeneration of the spectrum of the original complex, the redox process is ensured to have quantitative reversibility with one-electron transfer. Chemical oxidation was performed with Br_2, $FeCl_3$, and 2,3-dichloro-5,6-dicyanobenzoquinone, and the complete and efficient oxidation was achieved with $FeCl_3$ in a fivefold excess in dichloromethane. The oxidized species was quite stable during the course of reaction, and the conversion rate in controlled-potential oxidation at +1.0 V was more than 95% in reference to the chemical oxidation data. Fully reversible reduction was also carried out with a mild reducing agent such as potassium iodide. Electronic absorption spectra of the chemically and electrochemically oxidized species were identical, although the oxidized complex with $FeCl_3$ provided additional absorption due to $FeCl_3$. No further spectral change of the chemically oxidized species was observed with time in the concentration range from 10^{-5} to 10^{-4} M in both dichloromethane and benzene. This indicates that the monocationic complex exists as a monomer in solution. We, therefore, conclude that the one-electron oxidized species is the $[Mo^{VI}(O)(MEC)]^+$ ion. Alternatively overall redox reactions can be illustrated as in Scheme I, and the corresponding electronic spectral data are listed in Table II.

Substitution Reaction of Mo(O)(TPP)(MeO) with Monoanionic Ligands. Electronic absorption spectra of Mo(O)(TPP)(MeO), Mo(O)(TPP)(AcO), and Mo(O)(TPP)Cl (numbered as **1**, **2**, and **3**, respectively) are shown in Figure 4, and the corresponding spectral data are listed in Table III. We indicated previously that a ligand placed at the axial site trans to the oxo group of the Mo^V–octaethylporphine complex is labile, and Mo(O)(TPP)(EtO) shows two Soret-type bands in the 400–500-nm region in benzene, resulting from monomer ⇌ dimer equilibrium.[5] In order to clarify the coordination behavior of such axial ligands, we investigated the substitution reactions of **1** with acetate, chloride, and perchlorate ions (as X^-) as shown by eq 1.

$$Mo(O)(TPP)(MeO) + X^- \underset{k_{-1}}{\overset{k_1}{\rightleftharpoons}} Mo(O)(TPP)(X) + MeO^- \quad (1)$$

In a manner as reported previously for Mo(O)(TPP)(EtO), **1** exists almost exclusively as a monomer species in dichloromethane.[5] The Soret band, however, was split into two upon addition of chloride ion. Figure 5 shows the spectral change when the concentration of TEAC was varied from 0 to 0.5 M while that of **1** was maintained constant at 9.56×10^{-6} M; isosbestic points are observed at 427, 476, 560, and 628 nm. The equilibrium was reached instantaneously upon each addition of chloride ion, while the reaction proceeded rather slowly and the equilibria concerned were attained after ca. 20 h as for the addition of acetate and perchlorate ions. Concentrations of **1** and a substitution product, Mo(O)(TPP)(X), at various concentrations of added X^- ion can be evaluated from molar extinction coefficients for **1** and a substitution product, Mo(O)(TPP)(X), and observed optical densities, A_{obsd}. The ϵ_X values for Mo(O)(TPP)(X) species were determined by extrapolation of the A_{obsd} vs. $[X^-]^{-1}$ correlation curve to $[X^-]^{-1} \rightarrow 0$ as well as directly from the spectra of respective complexes. The ϵ_X values obtained by extrapolation and direct method are mutually in good agreement, i.e., 1.94×10^4 and 1.85×10^4 M^{-1} cm^{-1} at 455 nm, respectively, for X = Cl. The ϵ_X values graphically evaluated by extrapolation were used for calculations for the sake of reliability. Since X^- ion was present in a large excess relative to **1**, the following relation holds where $[X^-]_T$ stands for the total concentration

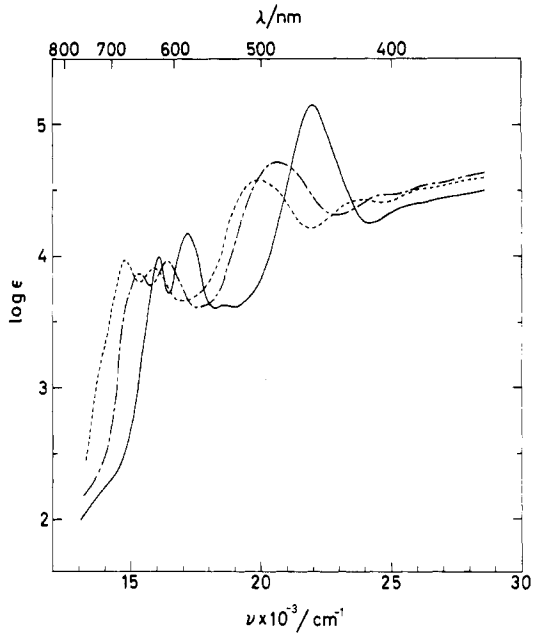

Figure 4. Electronic spectra of Mo^V porphyrins in dichloromethane at 25.0 ± 0.2 °C: —, Mo(O)(TPP)(MeO); -·-, Mo(O)(TPP)(AcO); ---, Mo(O)(TPP)Cl.

Table III. Electronic Absorption Bands (nm) for Mo(O)(TPP)(X) (X = MeO, AcO, and Cl) and Reduced Mo(O)(TPP)(MeO)[a]

Mo(O)-(TPP)(MeO) [in CH_2Cl_2–MeOH (50:1)][c]	Mo(O)-(TPP)(AcO) [in CH_2Cl_2–AcOH (50:1)][c]	Mo(O)-(TPP)(Cl)[b] [in CH_2Cl_2–TEAC (40:1)][c]	Mo^{IV}(O)-(TPP) [in CH_2Cl_2–TBAP (5.0×10^{-2} M)]
367 sh (27.3)	379 sh (36.0)	384 sh (34.0)	429 (295) (S)
393 sh (24.0)	411 sh (29.0)	418 (28.0)	480 sh (2.43)
455 (146) (S)	485 (52.6) (S)	503 (39.0) (S)	511 (3.79)
538 (4.31)	610 (9.41) (β)	630 (8.41) (β)	553 (17.2)
583 (15.3) (β)	653 (7.63) (α)	676 (9.70) (α)	590 (3.37)
623 (10.3) (α)		722 sh (2.3)	640 sh (1.2)
725 (0.17)			

[a] Measured at 25.0 ± 0.2 °C; molar absorption coefficients are given in parentheses after absorption bands as $\epsilon \times 10^{-3}$ (M^{-1} cm^{-1}); S, α, and β in parentheses stand for Soret, α, and β bands, respectively. [b] Molar absorption coefficients are given in the monomer unit. [c] Medium composition is given as molar ratio.

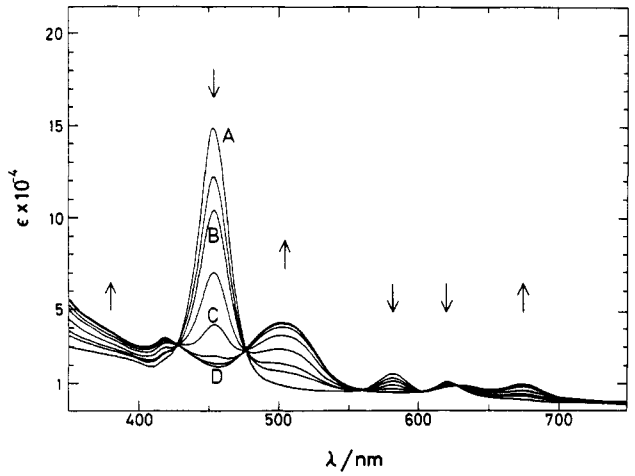

Figure 5. Electronic spectra of Mo(O)(TPP)(MeO) (9.56×10^{-6} M) in dichloromethane at 25.0 ± 0.1 °C in the presence of TEAC at various concentrations (0–5.05×10^{-1} M): A, 0 M; B, 3.53×10^{-3} M; C, 5.05×10^{-2} M; D, 5.05×10^{-1} M. Trends of absorption change are shown by arrows as TEAC concentration increases from A to D.

Table IV. Equilibrium Constants for Reactions of Mo(O)(TPP)(MeO) with Monoanionic Ligands in Dichloromethane at 25.0 ± 0.1 °C

monoanionic ligand[a]	aggregation status	K
Cl^-	dimer	0.1
AcO^-	monomer	6.3×10^{-3}
ClO_4^-	monomer	4.3×10^{-5}

[a] Reagents used as sources of monoanionic ligands are as follows: Cl^-, TEAC; AcO^-, acetic acid; ClO_4^-, TBAP.

of X^- ion and n represents the aggregation status; $n = 1$ for a monomer and $n = 2$ for a dimer.

$$[X^-]_T = [X^-] + n[\{Mo(O)(TPP)(X)\}_n] \simeq [X^-] \quad (2)$$

The equilibrium constants are given by eq 3 and 4 for the

$$K = k_1/k_{-1} = [Mo(O)(TPP)(X)]^2/[1][X^-]_T \quad (3)$$

$$K = [\{Mo(O)(TPP)(X)\}_2]^{3/2}/[1][X^-]_T \quad (4)$$

formation of the monomer and dimer species of Mo(O)(TPP)(X), respectively. Alternatively

$$\log [1] + \log [X^-]_T = 2 \log [Mo(O)(TPP)(X)] - \log K \quad (5)$$

$$\log [1] + \log [X^-]_T = \tfrac{1}{2} \log [\{Mo(O)(TPP)(X)\}_2] - \log K \quad (6)$$

Linear correlations between $\log [1] + \log [X^-]_T$ and $\log [Mo(O)(TPP)(X)]$ or $\log [\{Mo(O)(TPP)(X)\}_2]$ were observed with slopes of 1.4, 1.9, and 2.0 for X = Cl, AcO, and ClO_4, respectively, as shown in Figure 6. These results confirm that **3** exists as a dimer (**4**) while the others are monomeric species

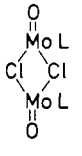

4

in dichloromethane. The equilibrium constants are listed in Table IV.

Electrochemical Behaviors of Mo(O)(TPP)(X). Figure 7 shows a typical cyclic voltammogram for **1**. Three large redox

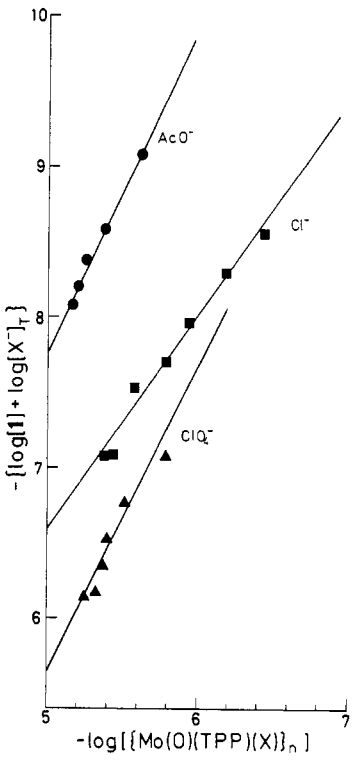

Figure 6. Determination of K values for reactions of **1** with monoanionic ligands (X^-'s) in dichloromethane at 25.0 ± 0.1 °C on the basis of eq 5 and 6: initial concentration of **1**, 10^{-5} M; X^-'s are shown in the figure.

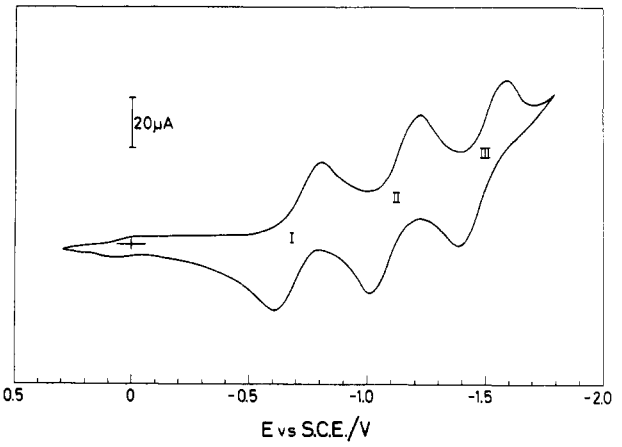

Figure 7. Cyclic voltammogram of Mo(O)(TPP)(MeO) (5.0×10^{-4} M) in dichloromethane containing 5.0×10^{-2} M TBAP at 23 °C (scan rate 100 mV s^{-1}).

couples indicated by I, II, and III as well as a small one near 0 V are observed for a potential range from 0.3 to −1.8 V vs. SCE. A linear relationship between i_p and $v^{1/2}$, identical values of i_{pa} and i_{pc}, and constant $E_{1/2}$ within an accuracy of ±3% were observed for each large redox couple. A potential separation between the anodic and cathodic peaks for each redox couple varied from 200 to 90 mV. These results are consistent with a typical reversible one-electron-transfer process, as in the case of Mo(O)(MEC). Substitution of the methoxo group of **1** with acetate or chloride ion resulted in a drastic anodic shift of peak I, while peaks II and III remained almost unchanged. These observations indicate that peak I is assigned to the redox of molybdenum (Mo^V/Mo^{IV}) and peaks II and III to successive one-electron redox processes of the porphyrin skeleton. The evaluated half-wave potentials for **1**–**3** are listed in Table V. When the voltammetric measurement of **1** (5.0×10^{-4} M) was carried out in the presence of 2.8×10^{-2} M

Table V. Redox Potentials for H_2TPP and Mo(V) Complexes in Dichloromethane at Room Temperature in the Presence of TBAP (5.0×10^{-2} M)[a]

compd[b]	temp, °C	metal		ligand		
		$E_{1/2}$Ox	$E_{1/2}$Red	$E_{1/2}$Ox	$E_{1/2}$Red(1)	$E_{1/2}$Red(2)
Mo(O)(MEC)	18	0.70	−0.72	1.3	<−2.0	
Mo(O)(TPP)(MeO)	26	(>1.7)	−0.74	(1.5)	−1.14	−1.49
Mo(O)(TPP)(AcO)[c]	26	(1.2)	−0.04	(1.5)	−1.11	−1.51
Mo(O)(TPP)(Cl)[d]	27	(1.3)	−0.06	(1.5)	−1.11	−1.50
H_2TPP	26			1.08	−1.23	−1.56

[a] $E_{1/2}$ values are given in V vs. SCE; values in parentheses were evaluated from cyclic voltammograms without confirmation of their structures by ESR spectroscopy. [b] Concentrations of all the compounds ca. 5.0×10^{-4} M. [c] 1 M AcOH added. [d] 9.0×10^{-3} M TEAC added.

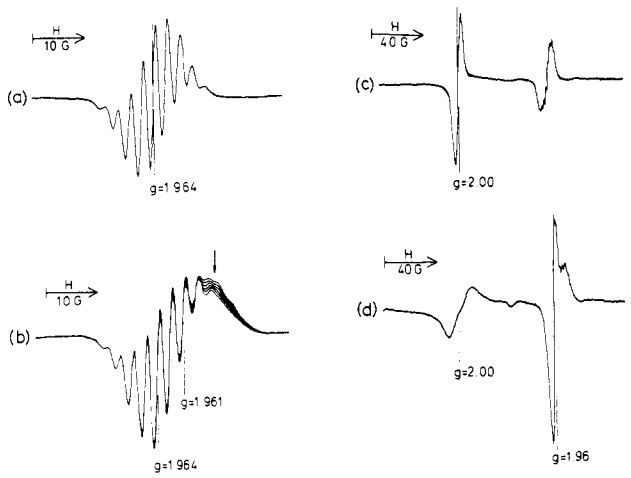

Figure 8. ESR spectra for the range of $I = 0$ during the electrochemical reduction of Mo(O)(TPP)(MeO) (2.0×10^{-3} M) in dichloromethane containing 0.10 M TBAP at room temperature: (a) before electrolysis; (b) reoxidation after complete electrolysis at −0.8 V vs. SCE, followed by reduction at −0.5 V vs. SCE (the region of signal decay is shown by an arrow); (c) reduction at −1.3 V vs. SCE (the signal due to **1** still remains for this reduction time); (d) reduction at −2.0 V vs. SCE.

TEAC as a supporting electrolyte, peak I became separated into two redox couples centered at −0.07 and −0.67 V vs. SCE in a potential range from 0.3 to −1.0 V vs. SCE, the ratio of peak currents, i_p(−0.07 V)/i_p(−0.67 V), being 2.3. When the TEAC concentration was raised to 5.4×10^{-2} M, the ratio increased to 3.3 even though the potentials of these waves remained unchanged. These two couples are assigned to the Mo^V/Mo^{IV} redox of **1** for −0.67 V and that of **3** for −0.07 V in reference to the data listed in Table V. Meanwhile, a small peak which appeared near 0 V (Figure 7) corresponds to the Mo^V/Mo^{IV} redox of Mo(O)(TPP)(ClO_4) formed from substitution reaction of **1** with perchlorate ion which was present in ca. 100-fold excess as a supporting electrolyte. As for **2** and **3**, peak I became rather complicated in the presence of TBAP as a supporting electrolyte because of the overlapping of redox peaks of the parent complexes with those of Mo(O)(TPP)(ClO_4) which was formed in a moderate amount. We, therefore, determined the accurate redox potentials of molybdenum involved in **2** and **3** by adding excess acetic acid and TEAC, respectively. Controlled-potential electrolysis of **1** was also studied by ESR spectroscopy. A dichloromethane solution of **1** (2.0×10^{-3} M) in the presence of TBAP (0.2 M) was electrochemically reduced at −0.8, −1.3, and −2.0 V vs. SCE, which are appropriate potentials for efficient performance of respective reductive one-electron-transfer reactions. When the reduction was carried out at −0.8 V vs. SCE, the signal due to **1** (Figure 8) was reduced with time and finally disappeared, no other signal being detected. This result indicates that peak I in the cyclic voltammogram (Figure 7) corresponds to the redox of molybdenum, Mo^V/Mo^{IV}, in

Scheme II

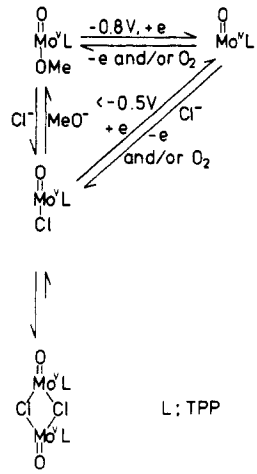

conformity with the previous assignment. After the reduction was stopped, a new signal having 11 superhyperfine lines due to ^{94}Mo, ^{96}Mo, ^{98}Mo, and ^{100}Mo(V) species appeared quickly, centered at $g = 1.962$–1.963 (Figure 8b). When the reduction potential was set at −0.5 V vs. SCE after such phenomenon, the intensity of nine lines at higher magnetic field region decreased and finally the signal converged into nine lines identical with those of the original complex. The observation shows that when a one-electron-reduced species, $[Mo^{IV}(O)(TPP)]^-$, was oxidized electrochemically or chemically with oxygen, two oxidized species were formed, i.e., parent complex **1** and **3**, the latter being formed from substitution reaction of **1** with chloride ion diffused out from the KCl salt bridge. The following facts are referred to for the formation of **3**: (1) a g value of the disappeared nine lines upon setting the reduction potential at −0.5 V is 1.961, which is identical with that of **3**; (2) a g value of **1** in dichloromethane saturated with dry HCl gas is also 1.961; (3) an equilibrium constant for the reaction between **1** and chloride ion is ca. 10^3-fold larger than that for the reaction between **1** and perchlorate ion; (4) $E_{1/2}$ of **3** for Mo^V/Mo^{IV} is −0.06 V vs. SCE. The redox behavior is illustrated in Scheme II.

When the reduction potential was maintained at −1.3 V vs. SCE, a new sharp signal due to radical species appeared at $g = 2.00$ and increased in intensity as the signal due to **1** decreased (Figure 8c). No hyperfine structure was observed in the new signal, characteristic of the π-anion radical of the porphyrin system.[19] The signal decayed immediately upon ceasing the reduction with concomitant increase of signal intensity due to **1**. When the potential was maintained at −2.0 V vs. SCE, the radical signal disappeared finally while another anisotropic signal caused by molybdenum nucleus appeared in a higher magnetic field region relative to that for **1**. The intensity of such an anisotropic signal ($g = 1.957$) increased slowly with time (Figure 8d); this would indicate the formation

(19) Felton, R. H.; Linschitz, H. *J. Am. Chem. Soc.* **1966**, *88*, 1113.

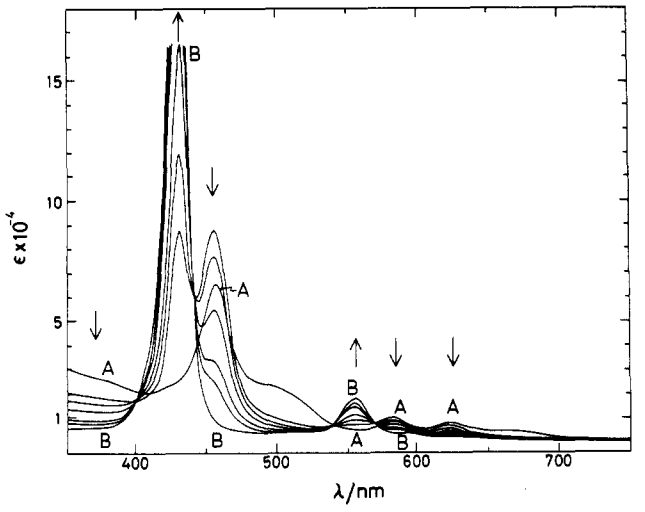

Figure 9. Electronic spectral change during the electrolytic reduction of Mo(O)(TPP)(MeO) (1.25×10^{-5} M) in dichloromethane containing 5.0×10^{-2} M TBAP at 15 °C: A, before reduction; B, after complete reduction. Trends of spectral change with time are shown by arrows.

Scheme III

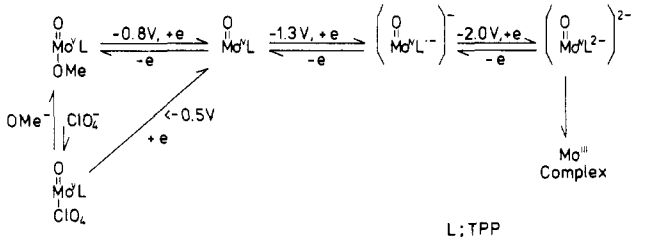

of Mo^{III} species. A weak signal observed at $g = 2.0$ after disappearance of the sharp radical signal seems to be associated with the above anisotropic signal. Electronic absorption spectra at various stages of electrolytic reduction of **1** at −1.0 V vs. SCE are shown in Figure 9. In an earlier stage of the reduction, the spectral change did not provide any isosbestic points. This must indicate the existence of more than two species: **1**, $Mo^{V}(O)(TPP)(ClO_4)$, and $Mo^{IV}(O)(TPP)$. A considerable amount of $Mo^{V}(O)(TPP)(ClO_4)$, which has a less negative reduction potential relative to **1**, was reduced more readily than **1**, generating $Mo^{IV}(O)(TPP)$. The spectral behavior provided clear isosbestic points at 399, 431, 536, and 569 nm after ca. 2 h of the reduction; the reduction proceeded exclusively from **1** to $Mo^{IV}(O)(TPP)$ through an one-electron-transfer process after the initial stage. The spectrum observed after completion of the electrolytic reduction was sufficiently identical with that for the complex obtained in chemical reduction with zinc–acetate acid in dichloromethane. More than 95% of **1** was electrochemically reduced at −1.0 V vs. SCE, and the reduced species, $Mo^{IV}(O)(TPP)$, was stable in solution at least for a few days under anaerobic conditions. After the reduction was stopped, a considerable amount of **3** was regenerated in addition to **1** in accord with the results of ESR measurements. The electrochemical redox behaviors of **1** are illustrated as in Scheme III.

Discussion

The recent X-ray crystallographic analysis indicates that **3** exists as a hexacoordinated mononuclear complex in the solid state, but the electronic spectrum in dichloromethane[6] is sufficiently identical with that reported by us here, indicating the change in coordination structure from a monomeric hexacoordinated one to dimeric heptacoordinated in solution. The large anodic shift of the reduction potential of molybdenum involved in **2** and **3** relative to that in **1** needs to be noted. As for the heptacoordinated structures **4** and **6**, the interactions

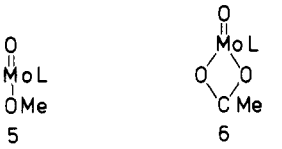

of d_{xz} and d_{yz} orbitals with σ orbitals of the axial ligand trans to the oxo group turn out to be important. These interactions would raise the energy levels of d_{xz} and d_{yz} orbitals and result in spreading of the d-electron cloud to give a nephelauxetic effect larger than that for the hexacoordinated complex (**5**). According to the X-ray crystallographic analysis of **3**, the Mo–Cl bond has an appreciable ionic character.[6] The magnitude of Mo=O stretching frequency for **3** (939 cm^{-1}) is considerably larger than that for **1** (906 cm^{-1}). These observations indicate that the Mo–OMe bond in **1** has larger covalent character which tends to increase the electron population at molybdenum; this is also reflected on A_{Mo} values (Table I). Consequently, these effects may lower the energy level of the d_{xy} orbital for **2** and **3**, and their reduction is facilitated compared with **1** while the oxidation of **1** at the molybdenum site is less facile than that of **2** and **3**.

In contrast to the large shift of reduction potential for molybdenum, no appreciable potential change was observed for formation of the radical anion (peak II) and the dianion (peak III) of the porphyrin ligand as seen in Table V. It is generally realized that the redox potential of a central metal is largely shifted, whereas those of planar ligands are hardly affected by the substitution of axial ligands for the complex coordinated with a planar macrocyclic ligand such as phthalocyanine.[20] We were unable to assign the redox potentials for H_3MEC, though it was obvious that Mo(O)(MEC) did not show any reduction potential for the corrole ligand in a cathodic region up to −2.0 V vs. SCE. The porphyrin ligand in Mo(O)(TPP)(X), however, has two successive one-electron reduction potentials at −1.1 and −1.5 V vs. SCE, a little shifted to the anodic side relative to H_2TPP. Owing to the lower skeletal symmetry of MEC, the separation between the lowest unoccupied (LUMO) and the highest occupied orbital (HOMO) of the macrocyclic ligand is expected to be larger in Mo(O)(MEC) than in Mo(O)(TPP)(X). This tends to render Mo(O)(MEC) less susceptible to reduction of the ligand as compared with Mo(O)(TPP)(X). The difference between the first and second reduction potentials for the porphyrin ligand is in the range of 0.35–0.40 V, which is comparable to those for other metalloporphyrins.[13] One criterion for distinguishing metal reduction from ligand reduction in metalloporphyrins, which apparently has a wide applicability, is that the numerical difference between the half-wave potentials for the first ligand oxidation and the first reduction, $\Delta E_{1/2}^{Ox/Red}$, is 2.25 ± 0.15 V.[13] This value, however, is as large as 2.73 V for Mo(O)(OEP)(OH);[13] OEP is octaethylporphyrin. We performed the voltammetric measurement of **1** up to +1.7 V vs. SCE as the extreme in the anodic region in dichloromethane and found the reversible one-electron redox couple at +1.5 V vs. SCE. This redox couple can be assigned to the first ligand oxidation for **1** since the separation from the first ligand-reduction potential for **1** is 2.64 V, comparable to that reported for Mo(O)(OEP)(OH). The reversible one-electron redox couple was found at +1.3 V vs. SCE for Mo(O)(MEC) in dichloromethane. By taking this redox couple as the first ligand-oxidation, we find that $\Delta E_{1/2}^{Ox/Red}$ is larger than 3.3 V. Thus, the energy separation between HOMO and LUMO

(20) Kadish, K. M.; Bottomley, L. A.; Cheng, J. S. *J. Am. Chem. Soc.* **1978**, *100*, 2731.

is larger in Mo(O)(MEC) than in Mo(O)(TPP)(X).

The Soret, α, and β bands of Mo(O)(MEC) were observed in regions lower by ca. 20 nm than the corresponding bands of molybdenum porphyrins. This seems to be consistent with the above discussion. The Soret, α, and β bands of the molybdenum porphyrin complexes depend on the nature of the axial ligand trans to the oxo group and are shifted to longer wavelength in the order MeO < AcO < Cl. Similar results have been obtained for the octaethylporphyrin complexes.[21] The value of $\Delta E_{1/2}^{Ox/Red}$ is independent of the nature of axial ligands, 0.35–0.40 V. This would indicate that the Soret, α, and β bands are not referred to exclusive $\pi-\pi^*$ transitions within ligand molecules but to intramolecular charge-transfer transitions such as a $a_{2u}a_{1u}(\pi) \rightarrow e_g(d\pi)$, at least in part. The energy levels of molybdenum d orbitals seem to be subjected to change by effective electronegativity of the metal. Less intense bands that appeared in the 500–600-nm region also reduced their intensities as the number of d electrons decreased from two to zero in regards to Mo(O)(MEC). The result further indicates that the less intense bands are primarily due to metal(d) → ligand(π^*) charge-transfer transitions. Although Mo(O)(MEC) and **1** have almost identical reduction potentials for the central molybdenum, the difference of their oxidation potentials is more than 1.0 V. Corrole serves as a trinegative ligand, so that Mo(V) ion binds the tetrapyrrolic ligand to form a square-pyramidal coordination structure with an oxo group at the top, the complex being electrically neutral. Since porphyrin is a dinegative ligand, the molybdenum(V) complex having an oxo group needs to take up another monoanionic ligand in order to satisfy electric neutrality. As mentioned above, the Mo–Cl bond in **3** has an appreciable ionic character; a positive charge localized at the molybdenum atom may facilitate the metal reduction. On the other hand, the Mo–OMe bond has a considerable covalent character, and, consequently, such a positive charge must be efficiently delocalized. This view is consistent with the fact that the molybdenum atom of **1** has a reduction potential identical with that of Mo(O)(MEC). Facile oxidation of the central molybdenum in Mo(O)(MEC) compared with **1** can be explained in terms of delocalization of the positive charge (formally on Mo) throughout the π-electron system involving the oxo group and the macrocyclic ligand via d_{xz} and d_{yz} orbitals since the Mo=O stretching vibration is greater for Mo(O)(MEC) than for **1**. In any case, the oxidation of molybdenum is more facile for Mo^V(O)(MEC) than for Mo^V–porphyrins due to the difference in charge density at the molybdenum atom as reflected on A_{Mo} values (Table I).

Mo^V(O)(MEC) has no coordination tendency at the axial site trans to the oxo group. The electronic absorption spectra of this complex measured in pyridine, tetrahydrofuran, dichloromethane, and dichloromethane–methanol were almost identical, and also the ESR spectrum in pyridine was identical with that measured in dichloromethane. These results suggest that the Mo=O bond is sufficiently strong, and the complex has a square-pyramidal structure with a molybdenum atom displaced from the ligand plane, so that the sixth coordination site has no practical coordination ability. Even though Mo(O)(TPP) takes up a monoanionic ligand at the site trans to the oxo group, this site is quite labile for substitution reaction. The molybdenum(V) ion has a strong affinity for oxygen, its hard acid character being reflected. Thus, an equilibrium for the reaction between **1** and chloride ion, a hard base, was achieved instantaneously, but the reaction of **1** with a more soft base, bromide ion, was too slow to obtain equilibrium constant.

Acknowledgment. We wish to thank Mr. H. Horiuchi, glassworker of our department, for his skill in preparing three-electrode cells used for controlled-potential electrolysis. This work was supported in part by the Asahi Glass Foundation for Industrial Technology.

Registry No. **1**, 74751-79-4; **2**, 77320-98-0; **3**, 77320-99-1; Mo(O)MEC, 63621-40-9; Mo(O)TPP(ClO_4), 77321-00-7; [Mo(O)(MEC)]$^-$, 74751-80-7; [Mo(O)(MEC)]$^+$, 74751-81-8; Mo^{IV}(O)TPP, 33519-60-7; H_3MEC, 73227-36-8; H_2TPP, 917-23-7.

(21) Gouterman, M. *Porphyrins* **1977**, *3*, Chapter 1.

Contribution from the Department of Inorganic Chemistry, Indian Association for the Cultivation of Science, Calcutta 700032, India

Chemistry of Ruthenium. 2.[1] Synthesis, Structure, and Redox Properties of 2-(Arylazo)pyridine Complexes

S. GOSWAMI, A. R. CHAKRAVARTY, and A. CHAKRAVORTY*

Received October 27, 1980

Two types of ruthenium(II) complexes RuX_2L_2 (green) and $[Ru(bpy)_2L](ClO_4)_2 \cdot H_2O$ (red) are reported (X = Cl, Br, I; L = 2-(phenylazo)pyridine or 2-(*m*-tolylazo)pyridine; bpy = 2,2′-bipyridine). The RuX_2L_2 species systematically displays single RuX and RuN(pyridine) stretches in the far IR, strongly suggesting a centrosymmetric configuration for the coordination sphere. Both types of complexes have intense $t_2(Ru) \rightarrow \pi^*(L)$ transitions in the visible region. $RuCl_2L_2$ is unreactive to Ag^+ and nitrogen bases; monodentate tertiary phosphines (P) however give $RuClPL_2^+$. Both RuX_2L_2 and $Ru(bpy)_2L^{2+}$ exhibit reversible or nearly reversible ruthenium(III)–ruthenium(II) couples at platinum electrode. The $E^\circ_{298}{}'$ values in acetonitrile are ~+0.9 V for $RuX_2L_2^+/RuX_2L_2$ and ~+1.60 V for $Ru(bpy)_2L^{3+}/Ru(bpy)_2L^{2+}$ vs. SCE. The azopyridine ligand system greatly stabilizes the +2 oxidation state in ruthenium. The complexes also display electrochemical responses on the negative side of SCE due to ligand-based reductions. Azo reduction occurs quasi-reversibly at ~−0.5 V in $Ru(bpy)_2L^{2+}$. The existence of a blue isomer of RuX_2L_2 (X = Cl, Br) having *cis*-RuX_2 is briefly noted.

Introduction

The ruthenium chemistry of chelating aromatic nitrogenous ligands has primarily grown around[2-7] pyridine bases, particularly 2,2′-bipyridine (bpy), and related species. In the course of a systematic search[1] for new ruthenium complexes,

(1) Part 1: Chakravarty, A. R.; Chakravorty, A. *Inorg. Chem.* **1981**, *20*, 275. See also: Chakravarty, A. R.; Chakravorty, A. *Inorg. Nucl. Chem. Lett.* **1979**, *15*, 307.

(2) Brown, G. M.; Krentzien, H. J.; Abe, M.; Taube, H. *Inorg. Chem.* **1979**, *18*, 3374. Callahan, R. W.; Keene, F. R.; Meyer, T. J.; Salmon, D. J. *J. Am. Chem. Soc.* **1977**, *99*, 1064.

(3) Dose, E. V.; Wilson, L. J. *Inorg. Chem.* **1978**, *17*, 2660.

0020-1669/81/1320-2246$01.25/0